

Measurements of exclusive B_s^0 decays at the $\Upsilon(5S)$

K. Abe,⁹ K. Abe,⁴⁹ I. Adachi,⁹ H. Aihara,⁵¹ D. Anipko,¹ K. Aoki,²⁵ T. Arakawa,³²
 K. Arinstein,¹ Y. Asano,⁵⁶ T. Aso,⁵⁵ V. Aulchenko,¹ T. Aushev,²¹ T. Aziz,⁴⁷ S. Bahinipati,⁴
 A. M. Bakich,⁴⁶ V. Balagura,¹⁵ Y. Ban,³⁷ S. Banerjee,⁴⁷ E. Barberio,²⁴ M. Barbero,⁸
 A. Bay,²¹ I. Bedny,¹ K. Belous,¹⁴ U. Bitenc,¹⁶ I. Bizjak,¹⁶ S. Blyth,²⁷ A. Bondar,¹
 A. Bozek,³⁰ M. Bračko,^{23,16} J. Brodzicka,^{9,30} T. E. Browder,⁸ M.-C. Chang,⁵⁰ P. Chang,²⁹
 Y. Chao,²⁹ A. Chen,²⁷ K.-F. Chen,²⁹ W. T. Chen,²⁷ B. G. Cheon,³ R. Chistov,¹⁵
 J. H. Choi,¹⁸ S.-K. Choi,⁷ Y. Choi,⁴⁵ Y. K. Choi,⁴⁵ A. Chuvikov,³⁹ S. Cole,⁴⁶ J. Dalseno,²⁴
 M. Danilov,¹⁵ M. Dash,⁵⁷ R. Dowd,²⁴ J. Dragic,⁹ A. Drutskoy,⁴ S. Eidelman,¹ Y. Enari,²⁵
 D. Epifanov,¹ S. Fratina,¹⁶ H. Fujii,⁹ M. Fujikawa,²⁶ N. Gabyshev,¹ A. Garmash,³⁹
 T. Gershon,⁹ A. Go,²⁷ G. Gokhroo,⁴⁷ P. Goldenzweig,⁴ B. Golob,^{22,16} A. Gorišek,¹⁶
 M. Grosse Perdekamp,^{11,40} H. Guler,⁸ H. Ha,¹⁸ J. Haba,⁹ K. Hara,²⁵ T. Hara,³⁵
 Y. Hasegawa,⁴⁴ N. C. Hastings,⁵¹ K. Hayasaka,²⁵ H. Hayashii,²⁶ M. Hazumi,⁹
 D. Heffernan,³⁵ T. Higuchi,⁹ L. Hinz,²¹ T. Hokuue,²⁵ Y. Hoshi,⁴⁹ K. Hoshina,⁵⁴ S. Hou,²⁷
 W.-S. Hou,²⁹ Y. B. Hsiung,²⁹ Y. Igarashi,⁹ T. Iijima,²⁵ K. Ikado,²⁵ A. Imoto,²⁶
 K. Inami,²⁵ A. Ishikawa,⁵¹ H. Ishino,⁵² K. Itoh,⁵¹ R. Itoh,⁹ M. Iwabuchi,⁶ M. Iwasaki,⁵¹
 Y. Iwasaki,⁹ C. Jacoby,²¹ M. Jones,⁸ H. Kakuno,⁵¹ J. H. Kang,⁵⁸ J. S. Kang,¹⁸
 P. Kapusta,³⁰ S. U. Kataoka,²⁶ N. Katayama,⁹ H. Kawai,² T. Kawasaki,³² H. R. Khan,⁵²
 A. Kibayashi,⁵² H. Kichimi,⁹ N. Kikuchi,⁵⁰ H. J. Kim,²⁰ H. O. Kim,⁴⁵ J. H. Kim,⁴⁵
 S. K. Kim,⁴³ T. H. Kim,⁵⁸ Y. J. Kim,⁶ K. Kinoshita,⁴ N. Kishimoto,²⁵ S. Korpar,^{23,16}
 Y. Kozakai,²⁵ P. Križan,^{22,16} P. Krokovny,⁹ T. Kubota,²⁵ R. Kulasiri,⁴ R. Kumar,³⁶
 C. C. Kuo,²⁷ E. Kurihara,² A. Kusaka,⁵¹ A. Kuzmin,¹ Y.-J. Kwon,⁵⁸ J. S. Lange,⁵
 G. Leder,¹³ J. Lee,⁴³ S. E. Lee,⁴³ Y.-J. Lee,²⁹ T. Lesiak,³⁰ J. Li,⁸ A. Limosani,⁹ C. Y. Lin,²⁹
 S.-W. Lin,²⁹ Y. Liu,⁶ D. Liventsev,¹⁵ J. MacNaughton,¹³ G. Majumder,⁴⁷ F. Mandl,¹³
 D. Marlow,³⁹ T. Matsumoto,⁵³ A. Matyja,³⁰ S. McOnie,⁴⁶ T. Medvedeva,¹⁵ Y. Mikami,⁵⁰
 W. Mitaroff,¹³ K. Miyabayashi,²⁶ H. Miyake,³⁵ H. Miyata,³² Y. Miyazaki,²⁵ R. Mizuk,¹⁵
 D. Mohapatra,⁵⁷ G. R. Moloney,²⁴ T. Mori,⁵² J. Mueller,³⁸ A. Murakami,⁴¹ T. Nagamine,⁵⁰
 Y. Nagasaka,¹⁰ T. Nakagawa,⁵³ I. Nakamura,⁹ E. Nakano,³⁴ M. Nakao,⁹ H. Nakazawa,⁹
 Z. Natkaniec,³⁰ K. Neichi,⁴⁹ S. Nishida,⁹ K. Nishimura,⁸ O. Nitoh,⁵⁴ S. Noguchi,²⁶
 T. Nozaki,⁹ A. Ogawa,⁴⁰ S. Ogawa,⁴⁸ T. Ohshima,²⁵ T. Okabe,²⁵ S. Okuno,¹⁷ S. L. Olsen,⁸
 S. Ono,⁵² W. Ostrowicz,³⁰ H. Ozaki,⁹ P. Pakhlov,¹⁵ G. Pakhlova,¹⁵ H. Palka,³⁰
 C. W. Park,⁴⁵ H. Park,²⁰ K. S. Park,⁴⁵ N. Parslow,⁴⁶ L. S. Peak,⁴⁶ M. Pernicka,¹³
 R. Pestotnik,¹⁶ M. Peters,⁸ L. E. Piilonen,⁵⁷ A. Poluektov,¹ F. J. Ronga,⁹ N. Root,¹
 J. Rorie,⁸ M. Rozanska,³⁰ H. Sahoo,⁸ S. Saitoh,⁹ Y. Sakai,⁹ H. Sakamoto,¹⁹ H. Sakaue,³⁴
 T. R. Sarangi,⁶ N. Sato,²⁵ N. Satoyama,⁴⁴ K. Sayeed,⁴ T. Schietinger,²¹ O. Schneider,²¹
 P. Schönmeier,⁵⁰ J. Schümann,²⁸ C. Schwanda,¹³ A. J. Schwartz,⁴ R. Seidl,^{11,40} T. Seki,⁵³
 K. Senyo,²⁵ M. E. Sevier,²⁴ M. Shapkin,¹⁴ Y.-T. Shen,²⁹ H. Shibuya,⁴⁸ B. Shwartz,¹
 V. Sidorov,¹ J. B. Singh,³⁶ A. Sokolov,¹⁴ A. Somov,⁴ N. Soni,³⁶ R. Stamen,⁹ S. Stanič,³³
 M. Starič,¹⁶ H. Stoeck,⁴⁶ A. Sugiyama,⁴¹ K. Sumisawa,⁹ T. Sumiyoshi,⁵³ S. Suzuki,⁴¹
 S. Y. Suzuki,⁹ O. Tajima,⁹ N. Takada,⁴⁴ F. Takasaki,⁹ K. Tamai,⁹ N. Tamura,³²
 K. Tanabe,⁵¹ M. Tanaka,⁹ G. N. Taylor,²⁴ Y. Teramoto,³⁴ X. C. Tian,³⁷ I. Tikhomirov,¹⁵

K. Trabelsi,⁹ Y. T. Tsai,²⁹ Y. F. Tse,²⁴ T. Tsuboyama,⁹ T. Tsukamoto,⁹ K. Uchida,⁸
 Y. Uchida,⁶ S. Uehara,⁹ T. Uglov,¹⁵ K. Ueno,²⁹ Y. Unno,⁹ S. Uno,⁹ P. Urquijo,²⁴
 Y. Ushiroda,⁹ Y. Usov,¹ G. Varner,⁸ K. E. Varvell,⁴⁶ S. Villa,²¹ C. C. Wang,²⁹
 C. H. Wang,²⁸ M.-Z. Wang,²⁹ M. Watanabe,³² Y. Watanabe,⁵² J. Wicht,²¹ L. Widhalm,¹³
 J. Wiechczynski,³⁰ E. Won,¹⁸ C.-H. Wu,²⁹ Q. L. Xie,¹² B. D. Yabsley,⁴⁶ A. Yamaguchi,⁵⁰
 H. Yamamoto,⁵⁰ S. Yamamoto,⁵³ Y. Yamashita,³¹ M. Yamauchi,⁹ Heyoung Yang,⁴³
 S. Yoshino,²⁵ Y. Yuan,¹² Y. Yusa,⁵⁷ S. L. Zang,¹² C. C. Zhang,¹² J. Zhang,⁹
 L. M. Zhang,⁴² Z. P. Zhang,⁴² V. Zhilich,¹ T. Ziegler,³⁹ A. Zupanc,¹⁶ and D. Zürcher²¹

(Belle Collaboration)

¹*Budker Institute of Nuclear Physics, Novosibirsk*

²*Chiba University, Chiba*

³*Chonnam National University, Kwangju*

⁴*University of Cincinnati, Cincinnati, Ohio 45221*

⁵*University of Frankfurt, Frankfurt*

⁶*The Graduate University for Advanced Studies, Hayama*

⁷*Gyeongsang National University, Chinju*

⁸*University of Hawaii, Honolulu, Hawaii 96822*

⁹*High Energy Accelerator Research Organization (KEK), Tsukuba*

¹⁰*Hiroshima Institute of Technology, Hiroshima*

¹¹*University of Illinois at Urbana-Champaign, Urbana, Illinois 61801*

¹²*Institute of High Energy Physics,*

Chinese Academy of Sciences, Beijing

¹³*Institute of High Energy Physics, Vienna*

¹⁴*Institute of High Energy Physics, Protvino*

¹⁵*Institute for Theoretical and Experimental Physics, Moscow*

¹⁶*J. Stefan Institute, Ljubljana*

¹⁷*Kanagawa University, Yokohama*

¹⁸*Korea University, Seoul*

¹⁹*Kyoto University, Kyoto*

²⁰*Kyungpook National University, Taegu*

²¹*Swiss Federal Institute of Technology of Lausanne, EPFL, Lausanne*

²²*University of Ljubljana, Ljubljana*

²³*University of Maribor, Maribor*

²⁴*University of Melbourne, Victoria*

²⁵*Nagoya University, Nagoya*

²⁶*Nara Women's University, Nara*

²⁷*National Central University, Chung-li*

²⁸*National United University, Miao Li*

²⁹*Department of Physics, National Taiwan University, Taipei*

³⁰*H. Niewodniczanski Institute of Nuclear Physics, Krakow*

³¹*Nippon Dental University, Niigata*

³²*Niigata University, Niigata*

³³*University of Nova Gorica, Nova Gorica*

³⁴*Osaka City University, Osaka*

³⁵*Osaka University, Osaka*

³⁶*Panjab University, Chandigarh*

- ³⁷*Peking University, Beijing*
- ³⁸*University of Pittsburgh, Pittsburgh, Pennsylvania 15260*
- ³⁹*Princeton University, Princeton, New Jersey 08544*
- ⁴⁰*RIKEN BNL Research Center, Upton, New York 11973*
- ⁴¹*Saga University, Saga*
- ⁴²*University of Science and Technology of China, Hefei*
- ⁴³*Seoul National University, Seoul*
- ⁴⁴*Shinshu University, Nagano*
- ⁴⁵*Sungkyunkwan University, Suwon*
- ⁴⁶*University of Sydney, Sydney NSW*
- ⁴⁷*Tata Institute of Fundamental Research, Bombay*
- ⁴⁸*Toho University, Funabashi*
- ⁴⁹*Tohoku Gakuin University, Tagajo*
- ⁵⁰*Tohoku University, Sendai*
- ⁵¹*Department of Physics, University of Tokyo, Tokyo*
- ⁵²*Tokyo Institute of Technology, Tokyo*
- ⁵³*Tokyo Metropolitan University, Tokyo*
- ⁵⁴*Tokyo University of Agriculture and Technology, Tokyo*
- ⁵⁵*Toyama National College of Maritime Technology, Toyama*
- ⁵⁶*University of Tsukuba, Tsukuba*
- ⁵⁷*Virginia Polytechnic Institute and State University, Blacksburg, Virginia 24061*
- ⁵⁸*Yonsei University, Seoul*

Abstract

Several exclusive B_s^0 decays are studied using a 1.86 fb^{-1} data sample collected at the $\Upsilon(5S)$ resonance with the Belle detector at the KEKB asymmetric energy e^+e^- collider. Combining the $B_s^0 \rightarrow D_s^{(*)-}\pi^+$, $B_s^0 \rightarrow D_s^{(*)-}\rho^+$, $B_s^0 \rightarrow J/\psi\phi$ and $B_s^0 \rightarrow J/\psi\eta$ decay modes, a significant B_s^0 signal is observed. The ratio $\sigma(e^+e^- \rightarrow B_s^*\bar{B}_s^*)/\sigma(e^+e^- \rightarrow B_s^{(*)}\bar{B}_s^{(*)}) = 0.94_{-0.09}^{+0.06}$ is obtained at the $\Upsilon(5S)$ energy, indicating that B_s^0 meson production proceeds predominantly through the creation of $B_s^*\bar{B}_s^*$ pairs. The B_s^0 and B_s^* meson masses are measured to be $M(B_s^0) = (5370 \pm 1 \pm 3) \text{ MeV}/c^2$ and $M(B_s^*) = (5418 \pm 1 \pm 3) \text{ MeV}/c^2$. Upper limits on the $B_s^0 \rightarrow \gamma\gamma$, $B_s^0 \rightarrow \phi\gamma$, $B_s^0 \rightarrow K^+K^-$ and $B_s^0 \rightarrow D_s^{(*)+}D_s^{(*)-}$ branching fractions are also reported.

PACS numbers: 13.20.Gd, 13.20.He, 13.25.Gv, 13.25.Hw, 14.40.Gx, 14.40.Nd

INTRODUCTION

A considerable B_s^0 production rate has been recently measured in e^+e^- collisions at the $\Upsilon(5S)$ energy [1, 2]. This suggests that exclusive B_s^0 decay studies at high luminosity e^+e^- B factories have great potential. Although several B_s^0 decay channels have been recently observed by the Tevatron experiments [3, 4], some B_s^0 decay modes can be better measured at e^+e^- colliders running at the $\Upsilon(5S)$ energy. The detectors taking data at the $\Upsilon(5S)$ have many advantages in studies of B_s^0 decays, such as high photon and π^0 reconstruction efficiency, trigger efficiency of almost 100% for hadronic modes and excellent charged kaon and pion identification. The possibility of partial reconstruction of specific B_s^0 decays and a model-independent determination of the number of initial B_s^0 mesons, which opens an opportunity for precise absolute B_s^0 branching fraction measurements, are additional advantages of B_s^0 studies at e^+e^- colliders running at the $\Upsilon(5S)$.

In this paper we report the measurements of exclusive B_s^0 decays based on a $\Upsilon(5S)$ data sample of 1.86 fb^{-1} , collected by the Belle detector [5] at the KEKB asymmetric energy e^+e^- collider [6]. This data sample is more than four times larger than the 0.42 fb^{-1} dataset collected at the $\Upsilon(5S)$ by the CLEO experiment in 2003 [7], where first evidence of exclusive B_s^0 decays at the $\Upsilon(5S)$ was found.

We fully reconstruct six modes $B_s^0 \rightarrow D_s^- \pi^+$, $B_s^0 \rightarrow D_s^{*-} \pi^+$, $B_s^0 \rightarrow D_s^- \rho^+$, $B_s^0 \rightarrow D_s^{*-} \rho^+$, $B_s^0 \rightarrow J/\psi \phi$ and $B_s^0 \rightarrow J/\psi \eta$, which have large reconstruction efficiencies and are described by unsuppressed tree diagrams. To improve the statistical significance of the B_s^0 signal, these six modes are combined; the masses of the B_s^0 and B_s^* mesons are determined from a common signal fit.

In addition, we search for several rare B_s^0 decays: the intrinsic penguin decay $B_s^0 \rightarrow \gamma\gamma$, the electromagnetic penguin decay $B_s^0 \rightarrow \phi\gamma$, and the hadronic penguin decay $B_s^0 \rightarrow K^+K^-$. Although the branching fractions for these decays are expected to be too small to be observed with this dataset, we can obtain competitive upper limits. To date only upper limits for the $B_s^0 \rightarrow \gamma\gamma$ [8] and $B_s^0 \rightarrow \phi\gamma$ [9] decays have been published. Within the Standard Model the $B_s^0 \rightarrow \gamma\gamma$ decay is expected to proceed via an intrinsic penguin diagram and the branching fraction is expected to be $(0.5 - 1.0) \times 10^{-6}$ [10, 11]. However, this decay is sensitive to some Beyond Standard Model (BSM) contributions and can be enhanced by one to two orders of magnitude in some BSM models [12, 13]. Although the process $B \rightarrow s\gamma$ provides a more restrictive constraint for many BSM models, in some models the $B_s^0 \rightarrow \gamma\gamma$ process is more sensitive [12, 13].

The decay modes $B_s^0 \rightarrow \phi\gamma$ and $B_s^0 \rightarrow K^+K^-$ are also described by penguin diagrams; these processes are natural processes in which to search for BSM physics [14, 15, 16, 17, 18]. The decay $B_s^0 \rightarrow K^+K^-$ has been observed by CDF using a simultaneous multi-channel analysis [19], where the overlapping signal peaks from $B_s^0 \rightarrow K^+K^-$, $B^0 \rightarrow K^+\pi^-$, $B^0 \rightarrow \pi^+\pi^-$ and $B_s^0 \rightarrow K^-\pi^+$ decay modes were separated statistically in the fit and the ratio $(f_s/f_d) \cdot \mathcal{B}(B_s^0 \rightarrow K^+K^-)/\mathcal{B}(B^0 \rightarrow K^+\pi^-) = 0.46 \pm 0.08 \pm 0.07$ was obtained.

Important results can also be obtained using $B_s^0 \rightarrow D_s^{(*)+} D_s^{(*)-}$ decay modes [20, 21]. These modes are expected to be predominantly CP eigenstates and, because their branching fractions are expected to be large, they should lead to a sizable lifetime difference between the CP -odd and CP -even B_s^0 mesons. Therefore within the SM framework the relative decay-width difference $\Delta\Gamma_{B_s^0}/\Gamma_{B_s^0}$ can be obtained from measurement of the $B_s^0 \rightarrow D_s^{(*)+} D_s^{(*)-}$ branching fractions.

BELLE DETECTOR AND EVENT SELECTION

The Belle detector operates at KEKB [6], an asymmetric energy double storage ring designed to collide 8 GeV electrons and 3.5 GeV positrons to produce $\Upsilon(4S)$ mesons with a boost of $\beta\gamma = 0.425$. In this analysis we use a data sample of 1.86 fb^{-1} taken at the $\Upsilon(5S)$ energy of $\sim 10869 \text{ MeV}$ with the same boost. The experimental conditions for data taking at the $\Upsilon(5S)$ are identical to those for $\Upsilon(4S)$ or continuum running.

Belle is a general-purpose large-solid-angle detector that consists of a three-layer Silicon Vertex Detector (SVD), a 50-layer Central Drift Chamber (CDC), an array of Aerogel Čerenkov Counters (ACC), a Time of Flight counter system (TOF), and a CsI(Tl) Electromagnetic Calorimeter (ECL) located inside a superconducting solenoidal coil with a 1.5 T magnetic field. An iron flux-return located outside the coil is instrumented to identify K_L^0 and muons (KLM). The detector is described in detail elsewhere [5]. A GEANT-based detailed simulation of the Belle detector is used to produce Monte Carlo event samples (MC) and determine efficiencies.

Charged tracks are required to have a momentum larger than $100 \text{ MeV}/c$. Kaon and pion mass hypotheses are assigned using a likelihood ratio $\mathcal{L}_{K/\pi} = \mathcal{L}_K / (\mathcal{L}_K + \mathcal{L}_\pi)$, obtained by combining information from the CDC (dE/dx), ACC, and TOF systems. We require $\mathcal{L}_{K/\pi} > 0.6$ ($\mathcal{L}_{K/\pi} < 0.6$) for kaon (pion) candidates [5]. With these requirements, the identification efficiency for particles used in this analysis varies from 86% to 91% (94% to 98%) for kaons (pions). A tighter kaon identification requirement $\mathcal{L}_{K/\pi} > 0.8$ is applied for the $B_s^0 \rightarrow K^+K^-$ decay, where the pion misidentification background is large.

Electrons are identified combining [22] information from the CDC (specific ionization dE/dx), the ACC, and the ECL (electromagnetic shower position, shape and energy). Muons are identified by matching to KLM hits and penetration depth [23].

ECL clusters with a photon-like shape, that are not associated with charged tracks, are accepted as photon candidates. Primary candidate photons (γ), that are used to reconstruct the $B_s^0 \rightarrow \phi\gamma$ and $B_s^0 \rightarrow \gamma\gamma$ decays, are required to have a proper bunch-crossing timing and to lie within the acceptance of the ECL barrel ($33^\circ < \theta_\gamma < 128^\circ$). To reduce the background from high-energy π^0 decays, where the two daughter photons are merged in a single cluster in the calorimeter, the ratio of the energy deposition in 3×3 ECL cells compared to that in 5×5 cells around the maximum energy ECL cell is required to exceed 95%. The main background sources of high energy photons are $\pi^0 \rightarrow \gamma\gamma$ and $\eta \rightarrow \gamma\gamma$ decays. To reduce these backgrounds, restrictions are imposed on the invariant mass of the candidate primary photon and any other photon (γ') in the event. The primary photon is rejected if $120 < M(\gamma\gamma') < 145 \text{ MeV}/c^2$ and $E_{\gamma'} > 30 \text{ MeV}$ or if $510 < M(\gamma\gamma') < 570 \text{ MeV}/c^2$ and $E_{\gamma'} > 200 \text{ MeV}$.

π^0 candidates are formed from pairs of photons, each with energy greater than 150 MeV , with an invariant mass within $\pm 15 \text{ MeV}/c^2$ (i.e. $\sim 3\sigma$, where $\sigma \sim 5 \text{ MeV}/c^2$ is the π^0 mass resolution) of the nominal π^0 mass. We reconstruct η mesons only in the clean $\eta \rightarrow \gamma\gamma$ mode, requiring an invariant mass to be within $\pm 20 \text{ MeV}/c^2$ ($\sim 2\sigma$) of the nominal η mass and photon energies to be larger than 50 MeV . K_S^0 candidates are formed from $\pi^+\pi^-$ pairs with an invariant mass within $\pm 10 \text{ MeV}/c^2$ ($\sim 3\sigma$) of the nominal K_S^0 mass and a common vertex displaced from the interaction point by more than 0.1 cm in the plane perpendicular to the beam direction.

Invariant masses for $\bar{K}^{*0} \rightarrow K^-\pi^+$ candidates are required to be within $\pm 50 \text{ MeV}/c^2$ of the nominal \bar{K}^{*0} mass; those of $\phi \rightarrow K^+K^-$ candidates, within $\pm 12 \text{ MeV}/c^2$ of the ϕ

mass. A $\pm 100 \text{ MeV}/c^2$ mass window is used to select ρ^+ candidates reconstructed in the $\rho^+ \rightarrow \pi^+\pi^0$ mode. D_s^+ mesons are reconstructed in the $\phi\pi^+$, $\bar{K}^{*0}K^+$ and $K_S^0K^+$ decay channels; all candidates must have a mass within $\pm 12 \text{ MeV}/c^2$ ($\sim 2.5\sigma$) of the nominal D_s^+ mass. The helicity angle distributions are expected to be proportional to $\cos^2\theta_{\text{hel}}^{D_s}$ for pseudoscalar-vector final states and the $|\cos\theta_{\text{hel}}^{D_s}| > 0.25$ requirement is applied for the $D_s^+ \rightarrow \phi\pi^+$ and $D_s^+ \rightarrow \bar{K}^{*0}K^+$ decays. The helicity angle $\theta_{\text{hel}}^{D_s}$ is defined as the angle between the directions of the K^+ and D_s^+ momenta in the ϕ rest frame (or the directions of the π^+ and D_s^+ momenta in the \bar{K}^{*0} rest frame in the case of $\bar{K}^{*0}K^+$ decay).

D_s^{*+} candidates are reconstructed in the $D_s^{*+} \rightarrow D_s^+\gamma$ mode, the measured D_s^{*+} and D_s^+ mass difference is required to be within $\pm 10 \text{ MeV}/c^2$ of its nominal value. The invariant mass of the candidate J/ψ meson is required to be within the range $|M(\mu^+\mu^-) - m_{J/\psi}| < 30 \text{ MeV}/c^2$ for the muon decay mode and within the asymmetric range $-100 < M(e^+e^-) - m_{J/\psi} < 30 \text{ MeV}/c^2$ for the electron decay mode, where $m_{J/\psi}$ is the nominal mass of the J/ψ meson.

Six B_s^0 decays to $D_s^-\pi^+$, $D_s^-\rho^+$, $D_s^{*-}\pi^+$, $D_s^{*-}\rho^+$, $J/\psi\phi$ and $J/\psi\eta$ final states and four rare B_s^0 decays to K^+K^- , $\phi\gamma$, $\gamma\gamma$ and $D_s^{(*)+}D_s^{(*)-}$ final states are reconstructed. The signals can be observed using two variables: the energy difference $\Delta E = E_{B_s^0}^{\text{CM}} - E_{\text{beam}}^{\text{CM}}$ and beam-constrained mass $M_{\text{bc}} = \sqrt{(E_{\text{beam}}^{\text{CM}})^2 - (p_{B_s^0}^{\text{CM}})^2}$, where $E_{B_s^0}^{\text{CM}}$ and $p_{B_s^0}^{\text{CM}}$ are the energy and momentum of the B_s^0 candidate in the e^+e^- center-of-mass (CM) system and $E_{\text{beam}}^{\text{CM}}$ is the CM beam energy. The B_s^0 mesons can be produced in e^+e^- collisions at the $\Upsilon(5S)$ energy via intermediate $B_s^*\bar{B}_s^*$, $B_s^*\bar{B}_s^0$, $B_s^0\bar{B}_s^*$ and $B_s^0\bar{B}_s^0$ channels, with $B_s^* \rightarrow B_s^0\gamma$. These intermediate channels can be distinguished kinematically in the M_{bc} and ΔE plane, where three well separated B_s^0 signal regions can be defined corresponding to the cases where both, only one, or none of the B_s^0 mesons originate from a B_s^* decay. These signal regions are defined as ellipses corresponding to $\pm(2.0-2.5)\sigma$ resolution intervals in M_{bc} and ΔE . A MC simulation of the studied B_s^0 decays indicate that the correlation between M_{bc} and ΔE is small and can be neglected in this analysis. The numbers of events inside and outside these regions can be used to estimate the number of B_s^0 signal and background events.

After all selections the dominant background is from $e^+e^- \rightarrow q\bar{q}$ continuum events ($q = u, d, s, \text{ or } c$). Topologically B_s^0 events are expected to be spherical, whereas the continuum events are expected to be jet-like. To suppress continuum background we exploit topological cuts, that were optimized using MC to model the signal and data outside the B_s^0 signal regions to estimate background. The ratio of the second to the zeroth Fox-Wolfram moments [24] is required to be less than 0.3 for the high background $D_s^{(*)-}\pi^+$, $D_s^{(*)-}\rho^+$ and K^+K^- final states, less than 0.5 for the $\gamma\gamma$ final state (to increase the signal efficiency of such non-spherical B_s^0 decays) and less than 0.4 for all the other final states. To suppress continuum further the angle θ_{thr}^* in the CM between the thrust axes of the particles forming the B_s^0 candidate and all other particles in the event is used. We require $|\cos\theta_{\text{thr}}^*| < 0.9$ for the low background final states with a J/ψ , $|\cos\theta_{\text{thr}}^*| < 0.7$ for the $D_s^{(*)-}\rho^+$ final states, $|\cos\theta_{\text{thr}}^*| < 0.6$ for B_s^0 events reconstructed using the $D_s^+ \rightarrow \bar{K}^{*0}K^+$ decay mode, $|\cos\theta_{\text{thr}}^*| < 0.5$ for the very high background K^+K^- final state and $|\cos\theta_{\text{thr}}^*| < 0.8$ for all the other final states.

STUDY OF $B_S^0 \rightarrow D_S^{(*)-}\pi^+$, $B_S^0 \rightarrow D_S^{(*)-}\rho^+$, $B_S^0 \rightarrow J/\psi\phi$ AND $B_S^0 \rightarrow J/\psi\eta$ DECAYS

The distribution in M_{bc} and ΔE for the $B_s^0 \rightarrow D_s^-\pi^+$ candidates is shown in Fig. 1a. Nine events are observed within the ellipsoidal B_s^0 signal region corresponding to the $B_s^*\bar{B}_s^*$

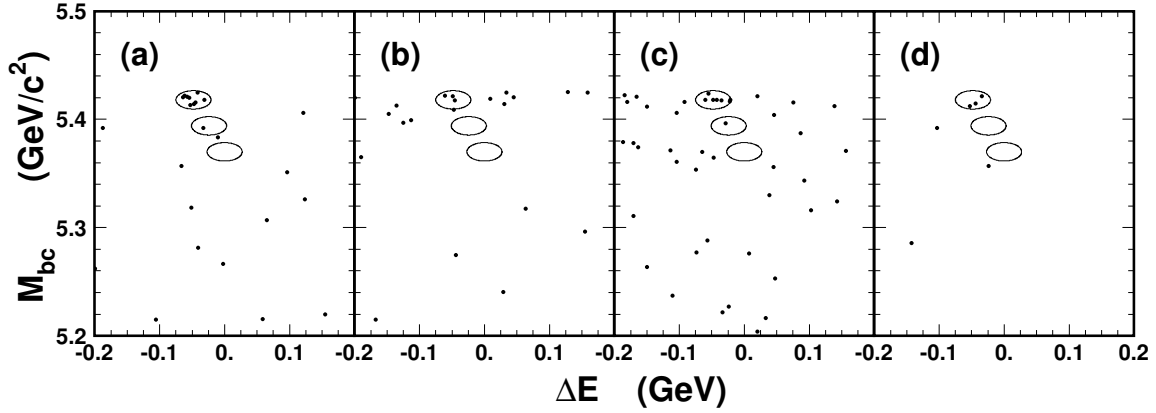


FIG. 1: The M_{bc} and ΔE scatter plots for the $B_s^0 \rightarrow D_s^+ \pi^-$ (a), $B_s^0 \rightarrow D_s^{*+} \pi^-$ (b), $B_s^0 \rightarrow D_s^{(*)+} \rho^-$ (c) and $B_s^0 \rightarrow J/\psi \phi$ and $B_s^0 \rightarrow J/\psi \eta$ (d) decay modes.

pair production channel. Only one event is observed in the B_s^0 signal region for the $B_s^* \bar{B}_s^0 + B_s^0 \bar{B}_s^*$ channels, and no events are observed for the $B_s^* \bar{B}_s^0$ channel. Background outside the signal region is small and corresponds to ~ 0.1 event in each of the three signal regions. The total number of $b\bar{b}$ events in the sample and the fraction of them containing B_s^0 mesons have been determined to be $N_{5S}^{b\bar{b}} = (5.61 \pm 0.03_{\text{stat}} \pm 0.29_{\text{syst}}) \times 10^5$ and $f_s = (18.0 \pm 1.3 \pm 3.2)\%$ [2]. Using these values, we measure the branching fraction $\mathcal{B}(B_s^0 \rightarrow D_s^- \pi^+) = (0.68 \pm 0.22 \pm 0.16)\%$. The systematic error includes the full $N_{5S}^{b\bar{b}}$ and f_s uncertainties and the uncertainty of $\sim 14\%$ in the reconstruction efficiency. This branching fraction is consistent with the value $(0.38 \pm 0.05 \pm 0.14)\%$, derived from a CDF measurement of $\mathcal{B}(B_s^0 \rightarrow D_s^- \pi^+)/\mathcal{B}(B^0 \rightarrow D^- \pi^+)$ [25] assuming the 2006 PDG values of the $B^0 \rightarrow D^- \pi^+$ and $D_s^- \rightarrow \phi \pi^-$ branching fractions [26].

M_{bc} and ΔE scatter plots are also obtained for the $B_s^0 \rightarrow D_s^{*-} \pi^+$ (Fig. 1b) and $B_s^0 \rightarrow D_s^{(*)-} \rho^+$ (Fig. 1c) decay modes. We observe four $B_s^0 \rightarrow D_s^{*-} \pi^+$ candidates and seven $B_s^0 \rightarrow D_s^{(*)-} \rho^+$ candidates in the $B_s^* \bar{B}_s^0$ channel, one $B_s^0 \rightarrow D_s^{(*)-} \rho^+$ candidate in the $B_s^* \bar{B}_s^0 + B_s^0 \bar{B}_s^*$ channel, and no candidates in the $B_s^0 \bar{B}_s^0$ channel.

The scatter plot in M_{bc} and ΔE for the $B_s^0 \rightarrow J/\psi \phi$ and $B_s^0 \rightarrow J/\psi \eta$ decays is shown in Fig. 1d. Two candidates are reconstructed in the $B_s^0 \rightarrow J/\psi \phi$ mode and one candidate is reconstructed in the $B_s^0 \rightarrow J/\psi \eta$ mode. One of the observed $B_s^0 \rightarrow J/\psi \phi$ candidates is reconstructed in the $J/\psi \rightarrow \mu^+ \mu^-$ mode and one in the $J/\psi \rightarrow e^+ e^-$ mode. As a cross-check, the branching fraction $\mathcal{B}(B_s^0 \rightarrow J/\psi \phi) = (0.9 \pm 0.6 \pm 0.2) \times 10^{-3}$ is obtained for these two candidates, which agrees with expectations within the large errors.

The six B_s^0 modes shown in Fig. 1 are combined to increase the statistical significance of the B_s^0 signal. Distributions in ΔE are obtained separately for events from three M_{bc} intervals, $5.408 < M_{bc} < 5.429 \text{ GeV}/c^2$ (Fig. 2a), $5.384 < M_{bc} < 5.405 \text{ GeV}/c^2$ (Fig. 2b) and $5.360 < M_{bc} < 5.380 \text{ GeV}/c^2$ (Fig. 2c), corresponding to B_s^0 production proceeding through the $B_s^* \bar{B}_s^*$, $B_s^* \bar{B}_s^0 + B_s^0 \bar{B}_s^*$ or $B_s^0 \bar{B}_s^0$ channels, respectively.

Each of these three distributions is fitted to the sum of a Gaussian to describe the signal and a linear function to describe background. In the $B_s^* \bar{B}_s^*$ channel (Fig. 2a), the width and the peak position are allowed to float, and their values $\sigma_{\Delta E} = (10.1 \pm 1.9) \text{ MeV}$ and $\langle \Delta E \rangle = (-47.8 \pm 2.6) \text{ MeV}$, respectively, are obtained from the fit. The width agrees with the value of $\sim 12 \text{ MeV}$, obtained from a MC simulation of the dominant $B_s^0 \rightarrow D_s^+ \pi^-$ decay

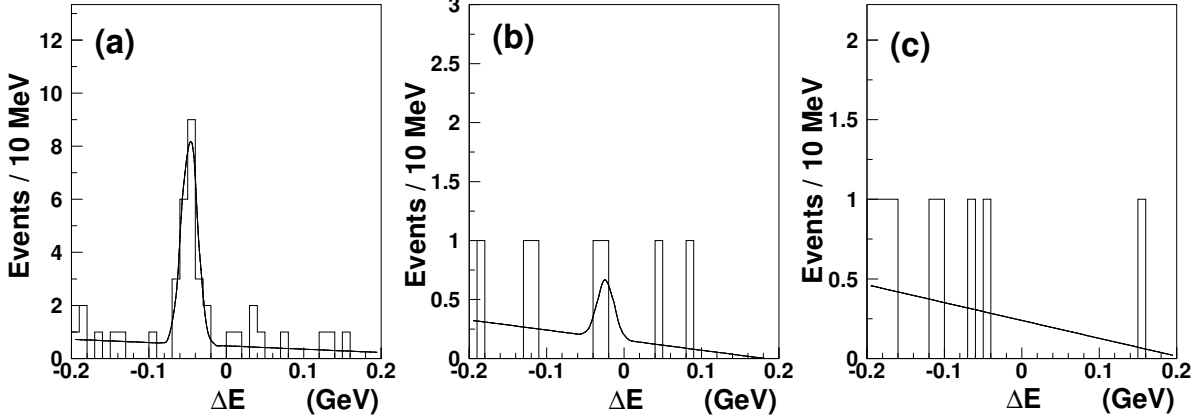


FIG. 2: The ΔE distributions for B_s^0 candidates with (a) $5.408 < M_{bc} < 5.429 \text{ GeV}/c^2$, (b) $5.384 < M_{bc} < 5.405 \text{ GeV}/c^2$ and (c) $5.360 < M_{bc} < 5.380 \text{ GeV}/c^2$, corresponding to B_s^0 production through the $B_s^* \bar{B}_s^*$, $B_s^* \bar{B}_s^0 + B_s^0 \bar{B}_s^*$ and $B_s^0 \bar{B}_s^0$ channels, respectively. Curves represent the results of the fits described in the text.

channel. Due to low statistics in the other two distributions, the peak positions and widths are fixed. The widths are taken from MC simulations. The peak position is fixed to zero for the $B_s^0 \bar{B}_s^0$ channel and that for the $B_s^* \bar{B}_s^0 + B_s^0 \bar{B}_s^*$ channel is fixed to -23.9 MeV , which is half of the value obtained for the $\langle \Delta E \rangle$ peak position in the $B_s^* \bar{B}_s^*$ channel. The fits yield 20.0 ± 4.8 events and 1.3 ± 2.0 events for the $B_s^* \bar{B}_s^*$ and $B_s^* \bar{B}_s^0 + B_s^0 \bar{B}_s^*$ channels, respectively; no events are observed in the $B_s^0 \bar{B}_s^0$ channel. From these numbers and approximately equal B_s^0 reconstruction efficiency in these three channels found in MC simulation, we obtain the ratio $\sigma(e^+e^- \rightarrow B_s^* \bar{B}_s^*) / \sigma(e^+e^- \rightarrow B_s^{(*)} \bar{B}_s^{(*)}) = 0.94_{-0.09}^{+0.06}$ at the $\Upsilon(5S)$ energy. Potential models predict the fraction of $B_s^* \bar{B}_s^*$ production to be around 70% [27, 28, 29].

The B_s^0 and B_s^* masses can be extracted from fits to the M_{bc} distributions of the observed signal events in the $B_s^* \bar{B}_s^*$ channel. In this channel the M_{bc} variable, calculated from the formula $M_{bc} = \sqrt{(E_{\text{beam}}^{\text{CM}})^2 - (p_{B_s^0}^{\text{CM}})^2}$, is equal, to a good approximation, to the mass of B_s^* meson. This follows from the fact that the difference between the B_s^0 and B_s^* momenta is statistically unbiased from zero and is smaller than the B_s^0 momentum experimental resolution. Figure 3a shows the M_{bc} distribution of the candidates in the range $-80 < \Delta E < -20 \text{ MeV}$, where signal events from $B_s^* \bar{B}_s^*$ production channel are expected. We fit this distribution with the sum of a Gaussian to describe the signal and the so-called ARGUS function [30] to describe background. The fit yields a mass value of $M(B_s^*) = (5418 \pm 1 \pm 3) \text{ MeV}/c^2$. The large systematic error is dominated by the uncertainty in the collider beam energy calibration resulting in a e^+e^- CM energy uncertainty of $\sim 5 \text{ MeV}$. The observed width of the B_s^* signal is $(3.6 \pm 0.6) \text{ MeV}/c^2$ and agrees with the value obtained from the MC simulation, which assumes zero natural width and is dominated by the KEKB energy spread.

Using the same B_s^0 candidates from the $-80 < \Delta E < -20 \text{ MeV}$ range we can also obtain the B_s^0 mass distribution (Fig. 3b), replacing the energy $E_{\text{beam}}^{\text{CM}}$ by the term $E_{\text{beam}}^{\text{CM}} - \langle \Delta E \rangle$ in the mass formula. The term $E_{\text{beam}}^{\text{CM}} - \langle \Delta E \rangle$ is approximately equal to the energy of B_s^0 meson, because the mean energy of the photon from the $B_s^* \rightarrow B_s^0 \gamma$ decay equals the $\langle \Delta E \rangle$ value. The photon energy is a constant in the B_s^* rest frame, and the small smearing effect due to the Lorentz transformation from the B_s^* rest frame to the CM rest

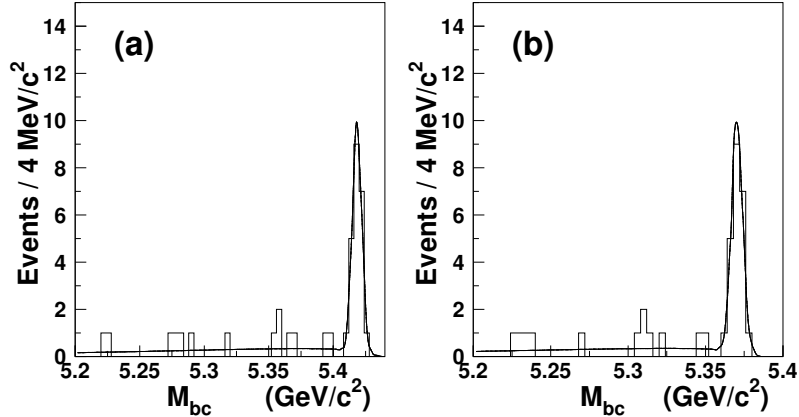


FIG. 3: The B_s^* (a) and B_s^0 (b) mass distributions for events within the $-0.08 < \Delta E < -0.02$ MeV interval, where the B_s^0 signal from the $B_s^* \bar{B}_s^*$ channel is expected. Curves represent the results of the fits described in the text.

frame does not bias the central value of the photon energy. The distribution shown in Fig. 3b is fitted to the sum of a Gaussian to describe the signal and the ARGUS function to describe background. The fit yields a mass value of $M(B_s^0) = (5370 \pm 1 \pm 3) \text{ MeV}/c^2$ and a width of $\sigma(B_s^0) = (3.6 \pm 0.6) \text{ MeV}/c^2$. The second uncertainty in the B_s^0 mass value is the systematic uncertainty due to the statistical uncertainty on the $\langle \Delta E \rangle$ measurement, which will be improved once more statistics will be available. The uncertainty due to the collider beam energy calibration nearby cancels in the $E_{\text{beam}}^{\text{CM}} - \langle \Delta E \rangle$ term. The obtained B_s^0 mass agrees well with the PDG value, $M(B_s^0) = (5369.6 \pm 2.4) \text{ MeV}/c^2$ [26], and the most recent CDF measurement, $M(B_s^0) = (5366.01 \pm 0.73 \pm 0.33) \text{ MeV}/c^2$ [31].

RARE DECAYS

Distributions in M_{bc} and ΔE are also obtained for reconstructed $B_s^0 \rightarrow \gamma\gamma$ (Fig. 4a), $B_s^0 \rightarrow \phi\gamma$ (Fig. 4b), $B_s^0 \rightarrow K^+K^-$ (Fig. 4c) and $B_s^0 \rightarrow D_s^{(*)+}D_s^{(*)-}$ (Fig. 4d) candidates. Only the B_s^0 signal regions corresponding to the dominant $B_s^* \bar{B}_s^*$ channel are considered for the searches reported here. These regions are wider for the $B_s^0 \rightarrow \phi\gamma$ and $B_s^0 \rightarrow \gamma\gamma$ decays, where the energy losses due to photon radiation lead to a large tail at lower values of ΔE . The shapes of the signal regions for these decays are optimized from the MC simulation.

No significant signals are observed in either of the plots shown in Fig. 4. However one $B_s^0 \rightarrow \phi\gamma$ event, two $B_s^0 \rightarrow K^+K^-$ events and one $B_s^0 \rightarrow D_s^{*+}D_s^-$ event lie within the signal regions, whereas backgrounds outside the signal regions are not large. The numbers of events within the signal regions, the estimated background contributions, the efficiencies, and the upper limits for the corresponding B_s^0 branching fractions are listed in Table 1. For comparison, the previously published upper limits are also shown. The numbers of events and the upper limits are obtained using only the B_s signal region corresponding to the $B_s^* \bar{B}_s^*$ channel. The upper limits are obtained using the Feldman-Cousins method [32], and a small correction due to systematic uncertainties is applied. The efficiencies are determined from the MC simulation. The number of initial $B_s^* \bar{B}_s^*$ pairs is obtained by multiplying the number of $B_s^{(*)} \bar{B}_s^{(*)}$ pairs measured in the inclusive analysis [2] by the production ratio of $B_s^* \bar{B}_s^*$ pairs to $B_s^{(*)} \bar{B}_s^{(*)}$ pairs obtained in this analysis.

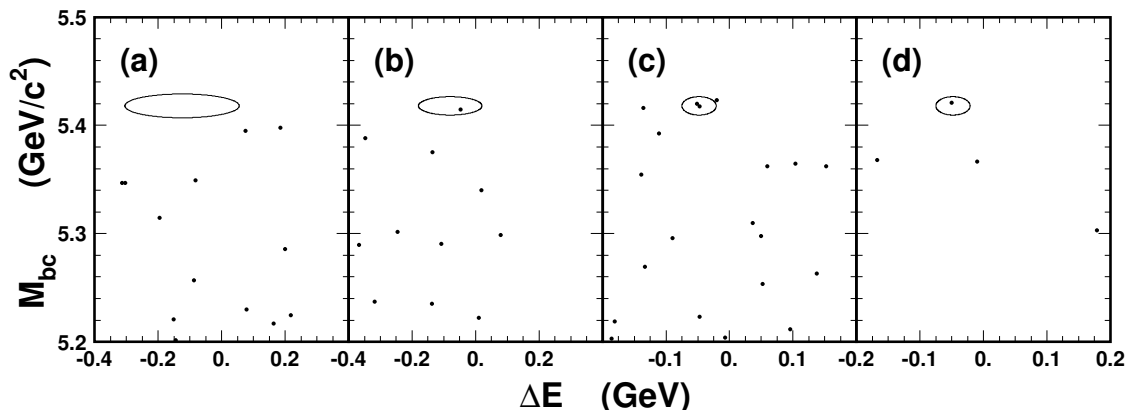


FIG. 4: The scatter plots in M_{bc} and ΔE for the $B_s^0 \rightarrow \gamma\gamma$ (a), $B_s^0 \rightarrow \phi\gamma$ (b), $B_s^0 \rightarrow K^+K^-$ (c) and $B_s^0 \rightarrow D_s^{(*)+}D_s^{(*)-}$ (d) decays. In the latter case, the signal event is reconstructed in the $B_s^0 \rightarrow D_s^{*+}D_s^-$ decay mode, while the three background events are reconstructed in the $B_s^0 \rightarrow D_s^+D_s^-$ decay mode. The ellipses indicate the B_s^0 signal regions for the $B_s^* \bar{B}_s^*$ channel.

TABLE I: The number of events in the signal region (Yield), the estimated background contribution (Bkg.), the efficiencies (Eff.) and the 90% C.L. upper limits derived in this analysis (This UL) and previously published (Prev. UL) for the $B_s^0 \rightarrow \gamma\gamma$, $B_s^0 \rightarrow \phi\gamma$, $B_s^0 \rightarrow K^+K^-$ and $B_s^0 \rightarrow D_s^{(*)+}D_s^{(*)-}$ decay modes.

Decay mode	Yield (events)	Bkg. (events)	Eff. (%)	This UL (10^{-4})	Prev. UL (10^{-4})
$B_s^0 \rightarrow \gamma\gamma$	0	0.5	20.0	0.53	1.48 [8]
$B_s^0 \rightarrow \phi\gamma$	1	0.15	5.9	3.9	1.2 [9]
$B_s^0 \rightarrow K^+K^-$	2	0.14	9.5	3.2	0.59 [33]
$B_s^0 \rightarrow D_s^+D_s^-$	0	0.02	0.020	670.	-
$B_s^0 \rightarrow D_s^{*+}D_s^-$	1	0.01	0.0099	1210.	-
$B_s^0 \rightarrow D_s^{*+}D_s^{*-}$	0	<0.01	0.0052	2570.	-

The obtained upper limit for the $B_s^0 \rightarrow \gamma\gamma$ decay is about three times smaller, than the current best value [8]. However, it is still two orders of magnitude above SM predictions. The upper limit obtained for $B_s^0 \rightarrow \phi\gamma$ is about a factor ten larger than the theoretically expected branching fraction. The upper limit obtained for the $B_s^0 \rightarrow K^+K^-$ decay is an order of magnitude larger than the value measured by CDF [19]. For SM branching fractions statistically significant signals of ~ 10 events can be obtained for the $B_s^0 \rightarrow \phi\gamma$ and $B_s^0 \rightarrow K^+K^-$ modes in a $\sim 30 \text{ fb}^{-1}$ dataset on the $\Upsilon(5S)$.

The upper limits obtained for $B_s^0 \rightarrow D_s^{(*)+}D_s^{(*)-}$ decays are of special interest because the $D_s^{(*)+}D_s^{(*)-}$ states are expected to be dominantly CP eigenstates. Assuming that the branching fractions for the $D_s^+D_s^-$, $D_s^{*+}D_s^-$, $D_s^+D_s^{*-}$ and $D_s^{*+}D_s^{*-}$ final states are each in the range (1–3)%, we expect about 5–10 events in each of these four channels with statistics of $\sim 30 \text{ fb}^{-1}$. Within the SM framework such measurements can provide an important constraint on the value of $\Delta\Gamma_{B_s^0}/\Gamma_{B_s^0}$.

CONCLUSIONS

Several exclusive B_s^0 decays are reconstructed in data taken at the $\Upsilon(5S)$ resonance with the Belle detector at the KEKB asymmetric energy e^+e^- collider. The 1.86 fb^{-1} data sample used in this analysis is currently the largest at the $\Upsilon(5S)$.

B_s^0 signals are found in six $B_s^0 \rightarrow D_s^{(*)-}\pi^+$, $B_s^0 \rightarrow D_s^{(*)-}\rho^+$, $B_s^0 \rightarrow J/\psi\phi$ and $B_s^0 \rightarrow J/\psi\eta$ decay modes. Combining these channels, we observe a significant B_s^0 signal and obtain the masses $M(B_s^0) = (5370 \pm 1 \pm 3)\text{ MeV}/c^2$ and $M(B_s^*) = (5418 \pm 1 \pm 3)\text{ MeV}/c^2$. B_s^0 production through the $B_s^*\bar{B}_s^*$ channel is found to dominate over other $B_s^{(*)}\bar{B}_s^{(*)}$ channels. The ratio $\sigma(e^+e^- \rightarrow B_s^*\bar{B}_s^*)/\sigma(e^+e^- \rightarrow B_s^{(*)}\bar{B}_s^{(*)}) = 0.94_{-0.09}^{+0.06}$ is measured. These results are in agreement with CLEO measurements [7].

We also searched for $B_s^0 \rightarrow \gamma\gamma$, $B_s^0 \rightarrow \phi\gamma$, $B_s^0 \rightarrow K^+K^-$ and $B_s^0 \rightarrow D_s^{(*)+}D_s^{(*)-}$ decay modes and set upper limits on their branching fractions. The upper limit on $B_s^0 \rightarrow \gamma\gamma$ is three times more restrictive than the best existing limit. The background levels in these decays are low, indicating that the sensitivity of future studies of these decays with larger statistics will not be limited by backgrounds. We expect that significant signals for $B_s^0 \rightarrow K^+K^-$, $B_s^0 \rightarrow \phi\gamma$ and $B_s^0 \rightarrow D_s^{(*)+}D_s^{(*)-}$ decays can be observed in $\sim 30\text{ fb}^{-1}$ of data. With such statistics the upper limit for the $B_s^0 \rightarrow \gamma\gamma$ decay will provide an important constraint on some BSM models.

We thank the KEKB group for the excellent operation of the accelerator, the KEK cryogenics group for the efficient operation of the solenoid, and the KEK computer group and the National Institute of Informatics for valuable computing and Super-SINET network support. We acknowledge support from the Ministry of Education, Culture, Sports, Science, and Technology of Japan and the Japan Society for the Promotion of Science; the Australian Research Council and the Australian Department of Education, Science and Training; the National Science Foundation of China and the Knowledge Innovation Program of the Chinese Academy of Sciences under contract No. 10575109 and IHEP-U-503; the Department of Science and Technology of India; the BK21 program of the Ministry of Education of Korea, the CHEP SRC program and Basic Research program (grant No. R01-2005-000-10089-0) of the Korea Science and Engineering Foundation, and the Pure Basic Research Group program of the Korea Research Foundation; the Polish State Committee for Scientific Research; the Ministry of Science and Technology of the Russian Federation; the Slovenian Research Agency; the Swiss National Science Foundation; the National Science Council and the Ministry of Education of Taiwan; and the U.S. Department of Energy.

-
- [1] M. Artuso *et al.* (CLEO Collaboration), Phys. Rev. Lett. **95**, 261801 (2005).
 - [2] K. Abe, *et al.* (Belle Collaboration), BELLE-CONF-0614, hep-ex/0608015.
 - [3] V. Papadimitriou, hep-ex/0511043.
 - [4] G. Gomez-Ceballos, hep-ex/0511009.
 - [5] A. Abashian *et al.* (Belle Collaboration), Nucl. Instr. and Meth. A **479**, 117 (2002).
 - [6] S. Kurokawa and E. Kikutani, Nucl. Instr. and Meth. A **499**, 1 (2003).
 - [7] G. Bonvicini *et al.* (CLEO Collaboration), Phys. Rev. Lett. **96**, 022002 (2006).
 - [8] M. Acciarri *et al.* (L3 Collaboration), Phys. Lett. B **363**, 137 (1995).
 - [9] D. Acosta *et al.* (CDF Collaboration), Phys. Rev. D **66**, 112002 (2002).
 - [10] L. Reina, G. Ricciardi and A. Soni, Phys. Rev. D **56**, 5805 (1997).

- [11] S. W. Bosch and G. Buchalla, JHEP 0208, 054 (2002).
- [12] A. Gemintern, S. Bar-Shalom and G. Eilam, Phys. Rev. D **70**, 035008 (2004).
- [13] W. J. Huo, C. D. Lu and Z. J. Xiao, hep-ph/0302177.
- [14] R. Fleischer, Phys. Lett. B **459**, 306 (1999).
- [15] A. Khodjamirian, T. Mannel and M. Melcher, Phys. Rev. D **68**, 114007 (2003).
- [16] D. London and J. Matias, Phys. Rev. D **68**, 114007 (2003).
- [17] A. J. Buras, R. Fleischer, S. Recksiegel and F. Schwab, Nucl. Phys. B **697**, 133 (2004).
- [18] S. Baek, D. London, J. Matias and J. Virto, JHEP 0602, 027 (2006).
- [19] A. Abulencia *et al.* (CDF Collaboration), hep-ex/0607021.
- [20] Y. Grossman, Phys. Lett. B **380**, 99 (1996).
- [21] I. Dunietz, R. Fleischer and U. Nierste, Phys. Rev. D **63**, 114015 (2001).
- [22] K. Hanagaki *et al.*, Nucl. Instr. and Meth. A **485**, 490 (2002).
- [23] A. Abashian *et al.*, Nucl. Instr. and Meth. A **491**, 69 (2002).
- [24] G. C. Fox and S. Wolfram, Phys. Rev. Lett. **41**, 1581 (1978).
- [25] A. Abulencia *et al.* (CDF Collaboration), Phys. Rev. Lett. **96**, 191801 (2006).
- [26] W.-M. Yao *et al.* (Particle Data Group), J. Phys. G **33**, 1 (2006).
- [27] N. Byers and D. S. Hwang, UCLA-87-TEP-44, 1987.
- [28] D. M. J. Lovelock *et al.* (CUSB Collaboration), Phys. Rev. Lett. **54**, 377 (1985).
- [29] J. Lee-Franzini *et al.* (CUSB Collaboration), Phys. Rev. Lett. **65**, 2947 (1990).
- [30] H. Albrecht *et al.* (ARGUS Collaboration), Phys. Lett. B **229**, 304 (1989).
- [31] D. Acosta *et al.* (CDF Collaboration), Phys. Rev. Lett. **96**, 202001 (2006).
- [32] G. J. Feldman and R. D. Cousins, Phys. Rev. D **57**, 3873 (1998).
- [33] D. Buskulic *et al.* (ALEPH Collaboration), Phys. Lett. B **384**, 471 (1996).